Multiscale Science and Engineering (2020) 2:257–275
https://doi.org/10.1007/s42493-020-00055-0

ORIGINAL RESEARCH

Dynamic Characterization of Structures from Limited Measurements Using a Subspace System Identification Method

Boyoung Kim[1] · **Jun Won Kang**[1] · **Keunhee Cho**[2]

Received: 13 October 2020 / Revised: 30 October 2020 / Accepted: 3 November 2020 / Published online: 18 November 2020

Abstract
In this study, we investigate a subspace-system identification method that estimates the modal characteristics and damping ratio of structures using a small number of sensor measurement responses. With this method, a Kalman state vector is first constructed from the input and measurement data, and then the state-space system matrix is optimized from it. For this purpose, a block Hankel matrix is constructed using the input data of the load applied to the structure and the measurement data of the response, and then the matrix is decomposed through QR factorization. Then, singular value decomposition is used to obtain the extended observability matrix and state-space system order n, and the state-space system matrix constituting the Kalman state vector is obtained via least-squares optimization. The natural frequency and damping ratio of the structural system are calculated from the eigenvalue of the obtained system matrix. To verify the effectiveness of this subspace state-space system identification method, the natural frequency and mode shape of a simply supported beam and cantilever beam were calculated using a limited number of measurement data, and the results were compared with an exact solution to evaluate the accuracy of the estimation results of the dynamic characteristics. Furthermore, the modal characteristics and damping ratio of a real bridge were estimated from acceleration data. The stability chart calculated from the example shows that the subspace state-space system identification method discussed in this study can accurately identify the modal characteristics of structures using only a small number of measurement data.

Keywords State-space system identification · Block Hankel matrix · Singular value decomposition · Modal characteristics · Stability chart

Introduction

System identification from the perspective of structural health monitoring is a computational method that uses measurement data to evaluate the dynamic characteristics and stability of structures. The increased length and flexibility of bridges has led to more frequent abnormal vibrations. Therefore, there is growing interest in evaluating the dynamic characteristics of structures in civil engineering. Recently, several studies on such system identification algorithms have been conducted, and one of the remarkable among them is a method to effectively estimate the higher mode natural frequency and mode shape of structures using a wireless measurement system [2].

Representative system identification methods using measurement data include the eigensystem realization algorithm (ERA) and subspace system identification (SSI). ERA obtains a state-space matrix from a Hankel matrix constructed using Markov parameters and computes the modal characteristics of a structure through eigenvalue analysis [7]. It is suitable for the system identification of structures with light damping and is effective with multiple input and output data. This method was extended to ERA-observer/Kalman filter identification (ERA-OKID), which extracts Markov parameters using the Observer Kalman filter considering the uncertainty of the structural response, and the ERA-natural excitation technique (ERA-NExT), which can solve the noise problem of input signals [3, 5, 6, 10]. ERA has been widely utilized to monitor aerospace and civil structures when sufficient input and output data are available. However, when using only the output response, the accuracy of system identification may be limited by the uncertainty in the data. Typically, to estimate the modal

✉ Jun Won Kang
jwkang@hongik.ac.kr

[1] Department of Civil Engineering, Hongik University, Seoul 04066, Korea

[2] Structural Engineering Research Institute, Korea Institute of Civil Engineering and Building Technology, Goyang-si, Gyeonggi-do 10223, Korea

characteristics of civil structures, it is necessary to use only output data. For bridges in particular, methods that utilize ambient vibration data without dynamic excitation are effective because the dynamic excitation of higher modes is difficult and vehicles must be controlled to acquire data [1]. SSI is generally known to have high reliability for estimating the modal characteristics of structures using only the output response [10]. A representative SSI technique is the numerical algorithm for subspace state-space system identification (N4SID) [11]. This method continuously projects the future output of a structure onto the past output and obtains a state-space system matrix through the correlation of the QR decomposition and coefficient matrices. It has the advantage of not requiring neither a priori knowledge about the order and observability indices of the system nor an iterative algorithm for non-linear optimization [8]. Owing to its high accuracy, achieved even when using only output data, despite the complexity of its detailed numerical computations, N4SID is suitable for estimating the dynamic characteristics of structures. This technique has been developed over the past decade, mainly for evaluating the health of aircraft elements. Still, its system-level application to large civil structures, such as bridges and buildings, remains an open issue [10].

In this study, we discuss the N4SID method, which is suitable only when ambient vibration is required, e.g., for bridges, and we evaluate its applicability to civil structures. In particular, we evaluate the accuracy of the dynamic characteristics of structural elements estimated using only a small number of sensor responses, and we estimate the modal characteristics and damping ratio of a real bridge using acceleration response field measurements. We also compare the system identification accuracy according to the measurement response type and discuss the validity of the system identification results estimated using the N4SID method through a stability chart.

The rest of this paper is structured as follows. In Sect. 2, we describe the state-space modeling of vibrating structures, and in Sect. 3, we describe the N4SID system identification algorithm and application procedure. In Sect. 4, we introduce a method for obtaining the modal characteristics and damping ratio via eigenvalue analysis of the identified system matrix. In Sect. 5, we evaluate the accuracy of the modal characteristics estimated using the N4SID through numerical examples and assess the applicability of the N4SID algorithm for the system identification of real bridges.

State-Space Modeling of Vibrating Structures

The equation of motion governing the dynamic behavior of a discrete structural system with n_d degrees of freedom is expressed as follows:

$$\mathbf{M}\ddot{\mathbf{U}}(t) + \mathbf{C}_0\dot{\mathbf{U}}(t) + \mathbf{K}\mathbf{U}(t) = \mathbf{F}(t) = \mathbf{B}_0\mathbf{u}(t) \tag{1}$$

where $\mathbf{M}$, $\mathbf{C}_0$, and $\mathbf{K} \in \mathbb{R}^{n_d \times n_d}$ are the mass matrix, damping matrix, and stiffness matrix of the structural system, respectively, and $\mathbf{F}(t) \in \mathbb{R}^{n_d \times 1}$ and $\mathbf{U}(t) \in \mathbb{R}^{n_d \times 1}$ are the load vector and displacement vector at time t, respectively. The load vector $\mathbf{F}(t)$ is expressed as the product of vector $\mathbf{u}(t) \in \mathbb{R}^{m \times 1}$ and matrix $\mathbf{B}_0 \in \mathbb{R}^{n_d \times m}$. The vector $\mathbf{u}(t)$ consists of m loads, which are a continuous function of time. The matrix $\mathbf{B}_0$ determines the position at which the load is input. Equation (1) can be transformed into the following state-space equation with $n(= 2n_d)$ variables:

$$\dot{\mathbf{x}}(t) = \mathbf{A}_c\mathbf{x}(t) + \mathbf{B}_c\mathbf{u}(t). \tag{2}$$

In Eq. (2), vector $\mathbf{x}(t)$ and matrices $\mathbf{A}_c$ and $\mathbf{B}_c$ are as follows:

$$\mathbf{x}(t) = \begin{bmatrix} \mathbf{U}(t) \\ \dot{\mathbf{U}}(t) \end{bmatrix} \tag{3}$$

$$\mathbf{A}_c = \begin{bmatrix} 0 & \mathbf{I} \\ -\mathbf{M}^{-1}\mathbf{K} & -\mathbf{M}^{-1}\mathbf{C}_0 \end{bmatrix} \tag{4}$$

$$\mathbf{B}_c = \begin{bmatrix} 0 \\ \mathbf{M}^{-1}\mathbf{B}_0 \end{bmatrix} \tag{5}$$

where $\mathbf{A}_c \in \mathbb{R}^{n \times n}$ is the state matrix of the system, $\mathbf{B}_c \in \mathbb{R}^{n \times m}$ is the input matrix, and $\mathbf{x}(t) \in \mathbb{R}^{n \times 1}$ is the state-space vector. From acceleration, velocity, and displacement measurements, the output vector of the system $\mathbf{y}(t) \in \mathbb{R}^{l \times 1}$ can be expressed as follows:

$$\mathbf{y}(t) = \mathbf{C}_a\ddot{\mathbf{U}}(t) + \mathbf{C}_v\dot{\mathbf{U}}(t) + \mathbf{C}_d\mathbf{U}(t) \tag{6}$$

where $\mathbf{C}_d$, $\mathbf{C}_v$, and $\mathbf{C}_a \in \mathbb{R}^{l \times n_d}$ are the output matrices for displacement, velocity, and acceleration, respectively. By calculating the acceleration $\ddot{\mathbf{U}}(t)$ and velocity $\dot{\mathbf{U}}(t)$ from Eq. (2) and substituting them in Eq. (6), the output response vector of the sensor can be expressed as follows:

$$\mathbf{y}(t) = \mathbf{C}\mathbf{x}(t) + \mathbf{D}\mathbf{u}(t) \tag{7}$$

In Eq. (7), $\mathbf{C} \in \mathbb{R}^{l \times n}$ is the output matrix multiplied by the state-space vector, and $\mathbf{D} \in \mathbb{R}^{l \times m}$ is a direct transmission matrix:

$$\mathbf{C} = \begin{bmatrix} \mathbf{C}_d - \mathbf{C}_a\mathbf{M}^{-1}\mathbf{K} & \mathbf{C}_v - \mathbf{C}_a\mathbf{M}^{-1}\mathbf{C}_0 \end{bmatrix} \tag{8}$$

$$\mathbf{D} = \mathbf{C}_a\mathbf{M}^{-1}\mathbf{B}_0 \tag{9}$$

Equations (2) and (7) are deterministic state-space equations that are continuous over time. When using acceleration data for system identification, $\mathbf{C}_a \neq 0$; therefore, the direct

transmission matrix $\mathbf{D}$ is included as part of the state-space model. However, when using the displacement or velocity response, $\mathbf{C}_a = 0$; therefore, in Eq. (7), $\mathbf{D} = 0$.

The actual response is measured at a discontinuous time ($t = k\Delta t, k \in \mathbb{N}$) with a certain time interval (Δt); in this case, the state-space model is expressed as follows:

$$\mathbf{x}_{k+1} = \mathbf{A}\mathbf{x}_k + \mathbf{B}\mathbf{u}_k, \tag{10}$$

$$\mathbf{y}_k = \mathbf{C}\mathbf{x}_k + \mathbf{D}\mathbf{u}_k \tag{11}$$

where $\mathbf{x}_k = \mathbf{x}(k\Delta t)$ is the state vector at time $t(= k\Delta t)$, $\mathbf{A} = \exp(\mathbf{A}_c \Delta t)$ is the discrete state matrix, and $\mathbf{B} = [\mathbf{A} - \mathbf{I}]\mathbf{A}_c^{-1}\mathbf{B}_c$ is the discrete input matrix [4]. Because real measurement signals always contain noise, a combined state-space model was constructed by adding an error term due to noise to the state-space model of discontinuous time:

$$\mathbf{x}_{k+1} = \mathbf{A}\mathbf{x}_k + \mathbf{B}\mathbf{u}_k + \mathbf{w}_k \tag{12}$$

$$\mathbf{y}_k = \mathbf{C}\mathbf{x}_k + \mathbf{D}\mathbf{u}_k + \mathbf{v}_k \tag{13}$$

where $\mathbf{w}_k \in \mathbb{R}^{n\times 1}$ is noise due to inaccurate modeling, and $\mathbf{v}_k \in \mathbb{R}^{l\times 1}$ is the measurement error caused by the inaccuracy of the sensors. The two terms cannot be measured and are assumed to be white noise with an average of zero. Then, the following covariance matrix can be constructed:

$$E\left[\begin{pmatrix}\mathbf{w}_p\\ \mathbf{v}_p\end{pmatrix}\begin{pmatrix}\mathbf{w}_q^T & \mathbf{v}_q^T\end{pmatrix}\right] = \begin{bmatrix}\mathbf{Q} & \mathbf{S}\\ \mathbf{S}^T & \mathbf{R}\end{bmatrix}\delta_{pq} \tag{14}$$

where E is the expected value operator, and δ_{pq} is the Kronecker delta. When performing system identification using the ambient vibration data of the structure, the input load value $\mathbf{u}_k$ is not measured; hence, the $\mathbf{u}_k$ term does not exist in Eqs. (12) and (13).

System Identification Using N4SID

N4SID uses the input load data $\mathbf{u}_k$ and measurement data $\mathbf{y}_k$ of the structure to construct the Kalman state vector, and derives the state-space system matrix using the least-squares method. Here, the Kalman state vector is obtained using the block Hankel matrix constructed using the input and measurement data.

Construction of a Block Hankel Matrix

Figure 1 shows the space–time structure of the response data measured in the discrete-time domain. The block Hankel matrix $\mathbf{H} \in \mathbb{R}^{2(m+l)i\times j}$ can be constructed with the submatrices of input data $\mathbf{u}_k$ and response data $\mathbf{y}_k$ measured at the k th time as shown in (15a):

$$\mathbf{H} = \frac{1}{\sqrt{j}}\begin{bmatrix}\mathbf{U}_{0|2i-1}\\ \mathbf{Y}_{0|2i-1}\end{bmatrix} \tag{15a}$$

$$\mathbf{U}_{0|2i-1} = \left[\begin{array}{cccc}\mathbf{u}_0 & \mathbf{u}_1 & \cdots & \mathbf{u}_{j-1}\\ \mathbf{u}_1 & \mathbf{u}_2 & \cdots & \mathbf{u}_j\\ \vdots & \vdots & \ddots & \vdots\\ \mathbf{u}_{i-1} & \mathbf{u}_i & \cdots & \mathbf{u}_{i+j-2}\\ \hline \mathbf{u}_i & \mathbf{u}_{i+1} & \cdots & \mathbf{u}_{i+j-1}\\ \mathbf{u}_{i+1} & \mathbf{u}_{i+2} & \cdots & \mathbf{u}_{i+j}\\ \vdots & \vdots & \ddots & \vdots\\ \mathbf{u}_{2i-1} & \mathbf{u}_{2i} & \cdots & \mathbf{u}_{2i+j-2}\end{array}\right] \tag{15b}$$

$$\mathbf{Y}_{0|2i-1} = \left[\begin{array}{cccc}\mathbf{y}_0 & \mathbf{y}_1 & \cdots & \mathbf{y}_{j-1}\\ \mathbf{y}_1 & \mathbf{y}_2 & \cdots & \mathbf{y}_j\\ \vdots & \vdots & \ddots & \vdots\\ \mathbf{y}_{i-1} & \mathbf{y}_i & \cdots & \mathbf{y}_{i+j-2}\\ \hline \mathbf{y}_i & \mathbf{y}_{i+1} & \cdots & \mathbf{y}_{i+j-1}\\ \mathbf{y}_{i+1} & \mathbf{y}_{i+2} & \cdots & \mathbf{y}_{i+j}\\ \vdots & \vdots & \ddots & \vdots\\ \mathbf{y}_{2i-1} & \mathbf{y}_{2i} & \cdots & \mathbf{y}_{2i+j-2}\end{array}\right] \tag{15c}$$

where the subscripts of $\mathbf{U}$ and $\mathbf{Y}$ indicate the subscripts of the first and last element vectors in the first column. When the block Hankel matrix is divided as above, $\mathbf{U}_{0|i-1}$ and $\mathbf{U}_{i|2i-1}$ are the past input and future input, respectively, and $\mathbf{Y}_{0|i-1}$ and $\mathbf{Y}_{i|2i-1}$ are the past output and future output, respectively.

QR Factorization

Using QR factorization, the Hankel matrix $\mathbf{H}$ in Eqs. (15a–15c) can be expressed as follows:

$$\mathbf{H} = \mathbf{R} \times \mathbf{Q}^T \tag{16}$$

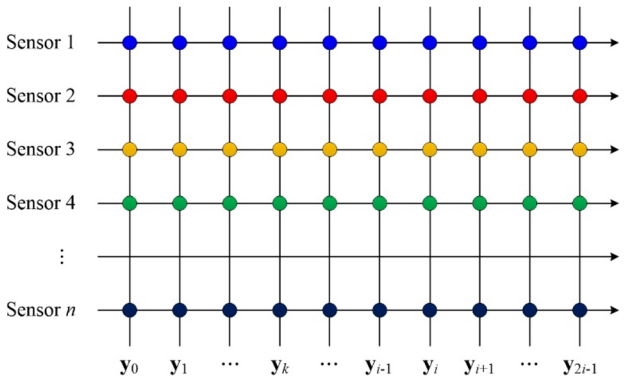

Fig. 1 Space–time structure of output vectors used for block Hankel matrix

where $\mathbf{R} \in \mathbb{R}^{2(m+l)i \times 2(m+l)i}$ is the lower triangular matrix, and $\mathbf{Q}^T \in \mathbb{R}^{2(m+l)i \times j}$ has an orthogonality of $\mathbf{Q}\mathbf{Q}^T = \mathbf{I}$. By dividing $\mathbf{R}$ and $\mathbf{Q}^T$ into submatrices, Eq. (16) can be expressed as follows:

$$\begin{array}{c} \\ mi \\ m \\ m(i-1) \\ li \\ l \\ l(i-1) \end{array} \begin{array}{c} \begin{array}{cccccc} mi & m & m(i-1) & li & l & l(i-1) \end{array} \\ \begin{bmatrix} \mathbf{U}_{0|i-1} \\ \mathbf{U}_{i|i} \\ \mathbf{U}_{i+1|2i-1} \\ \mathbf{Y}_{0|i-1} \\ \mathbf{Y}_{i|i} \\ \mathbf{Y}_{i+1|2i-1} \end{bmatrix} \end{array} = \begin{bmatrix} \mathbf{R}_{11} & 0 & 0 & 0 & 0 & 0 \\ \mathbf{R}_{21} & \mathbf{R}_{22} & 0 & 0 & 0 & 0 \\ \mathbf{R}_{31} & \mathbf{R}_{32} & \mathbf{R}_{33} & 0 & 0 & 0 \\ \mathbf{R}_{41} & \mathbf{R}_{42} & \mathbf{R}_{43} & \mathbf{R}_{44} & 0 & 0 \\ \mathbf{R}_{51} & \mathbf{R}_{52} & \mathbf{R}_{53} & \mathbf{R}_{54} & \mathbf{R}_{55} & 0 \\ \mathbf{R}_{61} & \mathbf{R}_{62} & \mathbf{R}_{63} & \mathbf{R}_{64} & \mathbf{R}_{65} & \mathbf{R}_{66} \end{bmatrix} \begin{bmatrix} \mathbf{Q}_1^T \\ \mathbf{Q}_2^T \\ \mathbf{Q}_3^T \\ \mathbf{Q}_4^T \\ \mathbf{Q}_5^T \\ \mathbf{Q}_6^T \end{bmatrix} \tag{17}$$

Projections

Projection refers to expression of the future output using the past and future input and past output. The projection of the future output can be defined as follows:

$$\mathbf{Z}_i = \mathbf{Y}_{i|2i-1} / \begin{bmatrix} \mathbf{U}_{0|2i-1} \\ \mathbf{Y}_{0|i-1} \end{bmatrix} \tag{18}$$

$$\mathbf{Z}_{i+1} = \mathbf{Y}_{i+1|2i-1} / \begin{bmatrix} \mathbf{U}_{0|2i-1} \\ \mathbf{Y}_{0|i} \end{bmatrix} \tag{19}$$

where $\mathbf{Z}_i$ and $\mathbf{Z}_{i+1}$ are the projection matrices of the future output based on the i th time and $i+1$ th time, respectively, and the projection operator is defined as $\mathbf{A}/\mathbf{B} = \mathbf{A}\mathbf{B}^T\left(\mathbf{B}\mathbf{B}^T\right)^{-1}\mathbf{B}$. This future output projection is the optimal predicted value of the future output $\mathbf{Y}_{i|2i-1}$ given the past and future input $\mathbf{U}_{0|2i-1}$ and past output $\mathbf{Y}_{0|i-1}$.

With N4SID, the system matrix is estimated using the projection matrices, $\mathbf{Z}_i$ and $\mathbf{Z}_{i+1}$, of the future output. This projection matrix of the future output can be constructed through the linear combination of the sub-block matrices of the block Hankel matrix comprising the input and measurement data as follows [9, 11]:

$$\mathbf{Z}_i = \mathbf{\Gamma}_i \hat{\mathbf{X}}_i + \mathbf{H}_i^d \mathbf{U}_{i|2i-1} \tag{20}$$

$$\mathbf{Z}_{i+1} = \mathbf{\Gamma}_{i-1} \hat{\mathbf{X}}_{i+1} + \mathbf{H}_{i-1}^d \mathbf{U}_{i+1|2i-1} \tag{21}$$

where $\mathbf{\Gamma}_i$ and $\mathbf{H}_i^d$ are the observability matrix and lower block triangular Toeplitz matrix, respectively, and consist of the system matrices $\mathbf{A}$, $\mathbf{B}$, $\mathbf{C}$, and $\mathbf{D}$ of the state-space equation. $\mathbf{\Gamma}_i$ and $\mathbf{H}_i^d$ are expressed as follows:

$$\mathbf{\Gamma}_i = \begin{bmatrix} \mathbf{C} \\ \mathbf{C}\mathbf{A} \\ \mathbf{C}\mathbf{A}^2 \\ \vdots \\ \mathbf{C}\mathbf{A}^{i-1} \end{bmatrix}, \tag{22}$$

$$\mathbf{H}_i^d = \begin{bmatrix} \mathbf{D} & 0 & 0 & \cdots & 0 \\ \mathbf{C}\mathbf{B} & \mathbf{D} & 0 & \cdots & 0 \\ \mathbf{C}\mathbf{A}\mathbf{B} & \mathbf{C}\mathbf{B} & \mathbf{D} & \cdots & 0 \\ \vdots & \vdots & \vdots & \ddots & \vdots \\ \mathbf{C}\mathbf{A}^{i-2}\mathbf{B} & \mathbf{C}\mathbf{A}^{i-3}\mathbf{B} & \mathbf{C}\mathbf{A}^{i-4}\mathbf{B} & \cdots & \mathbf{D} \end{bmatrix} \tag{23}$$

$\hat{\mathbf{X}}_i$ and $\hat{\mathbf{X}}_{i+1}$ are matrices representing a set of non-steady state Kalman filters. They are matrices with the estimated values of the state-space response considering the error at each time. These can be expressed using the system matrix and submatrix of the block Hankel matrix as follows [11]:

$$\hat{\mathbf{X}}_i = \begin{bmatrix} \mathbf{A}^i - \mathbf{Q}_i\mathbf{\Gamma}_i & \Delta_i^d - \mathbf{Q}_i\mathbf{H}_i^d & \mathbf{Q}_i \end{bmatrix} \begin{bmatrix} \mathbf{S}\mathbf{R}^{-1}\mathbf{U}_{0|2i-1} \\ \mathbf{U}_{0|i-1} \\ \mathbf{Y}_{0|i-1} \end{bmatrix} \tag{24}$$

$$\hat{\mathbf{X}}_{i+1} = \begin{bmatrix} \mathbf{A}^{i+1} - \mathbf{Q}_{i+1}\mathbf{\Gamma}_{i+1} & \Delta_{i+1}^d - \mathbf{Q}_{i+1}\mathbf{H}_{i+1}^d & \mathbf{Q}_{i+1} \end{bmatrix} \begin{bmatrix} \mathbf{S}\mathbf{R}^{-1}\mathbf{U}_{0|2i-1} \\ \mathbf{U}_{0|i} \\ \mathbf{Y}_{0|i} \end{bmatrix} \tag{25}$$

where $\mathbf{S}$ and $\mathbf{R}$ are matrices expressed by the past and future input and state-space response, respectively, and $\mathbf{Q}_i$ is a matrix expressed by these matrices and the system matrix [11]. The term Δ_i^d represents an extended controllability matrix, and is expressed as follows:

$$\Delta_i^d = \begin{bmatrix} \mathbf{A}^{i-1}\mathbf{B} & \mathbf{A}^{i-2}\mathbf{B} & \cdots & \mathbf{A}\mathbf{B} & \mathbf{B} \end{bmatrix} \tag{26}$$

Using Eqs. (20)–(21) and (24)–(25), the projection matrices $\mathbf{Z}_i$ and $\mathbf{Z}_{i+1}$ of the future output can be expressed as follows:

$$\mathbf{Z}_i = \begin{bmatrix} \mathbf{L}_i^1 & \mathbf{L}_i^2 & \mathbf{L}_i^3 \end{bmatrix} \begin{bmatrix} \mathbf{U}_{0|i-1} \\ \mathbf{U}_{i|2i-1} \\ \mathbf{Y}_{0|i-1} \end{bmatrix} \tag{27}$$

$$\mathbf{Z}_{i+1} = \begin{bmatrix} \mathbf{L}_{i+1}^1 & \mathbf{L}_{i+1}^2 & \mathbf{L}_{i+1}^3 \end{bmatrix} \begin{bmatrix} \mathbf{U}_{0|i} \\ \mathbf{U}_{i+1|2i-1} \\ \mathbf{Y}_{0|i} \end{bmatrix}. \tag{28}$$

In Eqs. (27) and (28), $\mathbf{L}_i^1$, $\mathbf{L}_i^2$, and $\mathbf{L}_i^3$ are expressed as follows:

$$\mathbf{L}_i^1 = \mathbf{\Gamma}_i \left(\left[\mathbf{A}^i - \mathbf{Q}_i\mathbf{\Gamma}_i \right] \mathbf{S} \left(\mathbf{R}^{-1} \right)_{1|mi} + \Delta_i^d - \mathbf{Q}_i\mathbf{H}_i^d \right) \tag{29}$$

$$\mathbf{L}_i^2 = \mathbf{H}_i^d + \mathbf{\Gamma}_i\left[\mathbf{A}^i - \mathbf{Q}_i\mathbf{\Gamma}_i\right]\mathbf{S}\left(\mathbf{R}^{-1}\right)_{mi+1|2mi} \tag{30}$$

$$\mathbf{L}_i^3 = \mathbf{\Gamma}_i\mathbf{Q}_i \tag{31}$$

where $\left(\mathbf{R}^{-1}\right)_{1|mi}$ is the submatrix from column 1 to column mi. To express the projection matrix of the future output, $\mathbf{L}_i^1$, $\mathbf{L}_i^2$, and $\mathbf{L}_i^3$ can be theoretically expressed using the system matrix as above. However, when using measurement data, Eqs. (17)–(19) are used for approximation as follows [11]:

$$\mathbf{Z}_i = \mathbf{Y}_{i|2i-1} / \begin{bmatrix} \mathbf{U}_{0|2i-1} \\ \mathbf{Y}_{0|i-1} \end{bmatrix} = \begin{bmatrix} \mathbf{L}_i^1 & \mathbf{L}_i^2 & \mathbf{L}_i^3 \end{bmatrix} \begin{bmatrix} \mathbf{U}_{0|i-1} \\ \mathbf{U}_{i|2i-1} \\ \mathbf{Y}_{0|i-1} \end{bmatrix} = \mathbf{R}_{5:6,1:4}\mathbf{R}_{1:4,1:4}^{-1} \begin{bmatrix} \mathbf{U}_{0|2i-1} \\ \mathbf{Y}_{0|i-1} \end{bmatrix} \tag{32}$$

$$\mathbf{Z}_{i+1} = \mathbf{Y}_{i+1|2i-1} / \begin{bmatrix} \mathbf{U}_{0|2i-1} \\ \mathbf{Y}_{0|i} \end{bmatrix} = \begin{bmatrix} \mathbf{L}_{i+1}^1 & \mathbf{L}_{i+1}^2 & \mathbf{L}_{i+1}^3 \end{bmatrix} \begin{bmatrix} \mathbf{U}_{0|i} \\ \mathbf{U}_{i+1|2i-1} \\ \mathbf{Y}_{0|i} \end{bmatrix} = \mathbf{R}_{6:6,1:5}\mathbf{R}_{1:5,1:5}^{-1} \begin{bmatrix} \mathbf{U}_{0|2i-1} \\ \mathbf{Y}_{0|i} \end{bmatrix} \tag{33}$$

Singular Value Decomposition

According to Eqs. (29) and (31), the column space of $\mathbf{L}_i^1$ and $\mathbf{L}_i^3$ is the same as the column space of $\mathbf{\Gamma}_i$. The column space of a matrix is a subspace that can consist of linearly independent column vectors of that matrix. This means that the observability matrix $\mathbf{\Gamma}_i$ and system order n can be determined from the column space of these matrices. In this study, they are determined according to the following procedure [11]:

- Equations (20) and (21), which are the projection matrices of the future output, are reconstructed as follows:

$$\hat{\mathbf{X}}_i = \mathbf{\Gamma}_i^{\dagger}\left[\mathbf{Z}_i - \mathbf{H}_i^d\mathbf{U}_{i|2i-1}\right] \tag{34}$$

$$\hat{\mathbf{X}}_{i+1} = \mathbf{\Gamma}_{i-1}^{\dagger}\left[\mathbf{Z}_{i+1} - \mathbf{H}_{i-1}^d\mathbf{U}_{i+1|2i-1}\right] \tag{35}$$

  where $\mathbf{\Gamma}_i^{\dagger}$ is the Moore–Penrose pseudo-inverse matrix of $\mathbf{\Gamma}_i$. $\mathbf{\Gamma}_i\hat{\mathbf{X}}_i$ is the result of subtracting $\mathbf{H}_i^d\mathbf{U}_{i|2i-1}$ from the projection response matrix $\mathbf{Z}_i$ and can be approximated using Eqs. (27) and (30) as follows:

$$\mathbf{\Gamma}_i\hat{\mathbf{X}}_i \approx \mathbf{Z}_i - \mathbf{L}_i^2\mathbf{U}_{i|2i-1} = \begin{bmatrix} \mathbf{L}_i^1 & 0 & \mathbf{L}_i^3 \end{bmatrix} \begin{bmatrix} \mathbf{U}_{0|i-1} \\ \mathbf{U}_{i|2i-1} \\ \mathbf{Y}_{0|i-1} \end{bmatrix} \tag{36}$$

- From Eq. (17), by performing singular value decomposition, Eq. (36) is expressed as follows:

$$\begin{aligned} \mathbf{\Gamma}_i\hat{\mathbf{X}}_i &\approx \begin{bmatrix} \mathbf{L}_i^1 & 0 & \mathbf{L}_i^3 \end{bmatrix} \begin{bmatrix} \mathbf{U}_{0|i-1} \\ \mathbf{U}_{i|2i-1} \\ \mathbf{Y}_{0|i-1} \end{bmatrix} \\ &= \begin{bmatrix} \mathbf{L}_i^1 & 0 & \mathbf{L}_i^3 \end{bmatrix} \mathbf{R}_{1:4,1:4}\mathbf{Q}_{1:4}^T \\ &= \begin{bmatrix} \mathbf{U}_1 & \mathbf{U}_2 \end{bmatrix} \begin{bmatrix} \mathbf{\Sigma}_1 & 0 \\ 0 & \mathbf{\Sigma}_2 \end{bmatrix} \mathbf{V}^T\mathbf{Q}_{1:4}^T \end{aligned} \tag{37}$$

  When $\mathbf{\Gamma}_i\hat{\mathbf{X}}_i$ is rank-deficient, the singular value matrix is divided into a non-zero part and a zero part. In the above equation, $\mathbf{\Sigma}_1$ is a singular value matrix with a non-zero diagonal component, and $\mathbf{\Sigma}_2$ is a singular value matrix with a diagonal component of zero. Because n is the rank of $\mathbf{\Gamma}_i\hat{\mathbf{X}}_i$ (the number of rows of the Kalman filter $\hat{\mathbf{X}}_i$ is equal to the state-space system order n), the size of $\mathbf{\Sigma}_1$ is equal to the system order n.
- Because the column spaces of $\mathbf{\Gamma}_i$ and $\mathbf{U}_1\mathbf{\Sigma}_1^{1/2}$ are identical, $\mathbf{\Gamma}_i$ can be obtained as follows:

$$\mathbf{\Gamma}_i = \mathbf{U}_1\mathbf{\Sigma}_1^{1/2} \tag{38}$$

  where $\mathbf{\Gamma}_{i-1}$ is

$$\mathbf{\Gamma}_{i-1} = \underline{\mathbf{\Gamma}}_i \tag{39}$$

  l is the number of measurements, and $\underline{\mathbf{\Gamma}}_i$ is the matrix excluding the last l rows in $\mathbf{\Gamma}_i$.

Calculation of System Matrices

The non-steady state Kalman filter matrices $\hat{\mathbf{X}}_i$ are $\hat{\mathbf{X}}_{i+1}$, constructed at time t_i and t_{i+1}, satisfy the following equation [11]:

$$\begin{bmatrix} \hat{\mathbf{X}}_{i+1} \\ \mathbf{Y}_{i|i} \end{bmatrix} = \begin{bmatrix} \mathbf{A} \\ \mathbf{C} \end{bmatrix} \hat{\mathbf{X}}_i + \begin{bmatrix} \mathbf{B} \\ \mathbf{D} \end{bmatrix} \mathbf{U}_{i|i} + \begin{bmatrix} \mathbf{U}_{0|2i-1} \\ \mathbf{Z}_i \\ \hat{\mathbf{X}}_i \end{bmatrix}^{\perp} \tag{40}$$

Equations (34) and (35) can be substituted into the Kalman filter equation above to obtain the following equation:

$$\begin{bmatrix} \boldsymbol{\Gamma}_{i-1}^{\dagger}\mathbf{Z}_{i+1} \\ \mathbf{Y}_{i|i} \end{bmatrix} = \begin{bmatrix} \mathbf{A} \\ \mathbf{C} \end{bmatrix} \boldsymbol{\Gamma}_i^{\dagger}\mathbf{Z}_i + \begin{bmatrix} \mathbf{K}_{12} \\ \mathbf{K}_{22} \end{bmatrix} \mathbf{U}_{i|2i-1} + \begin{bmatrix} \mathbf{U}_{0|2i-1} \\ \mathbf{Z}_i \\ \widehat{\mathbf{X}}_i \end{bmatrix}^{\perp} \tag{41}$$

This can then be further transformed as follows:

$$\begin{bmatrix} \boldsymbol{\Gamma}_{i-1}^{\dagger}\mathbf{Z}_{i+1} \\ \mathbf{Y}_{i|i} \end{bmatrix} = \begin{bmatrix} \mathbf{A} & \mathbf{K}_{12} \\ \mathbf{C} & \mathbf{K}_{22} \end{bmatrix} \begin{bmatrix} \boldsymbol{\Gamma}_i^{\dagger}\mathbf{Z}_i \\ \mathbf{U}_{i|2i-1} \end{bmatrix} + \begin{bmatrix} \mathbf{U}_{0|2i-1} \\ \mathbf{Z}_i \\ \widehat{\mathbf{X}}_i \end{bmatrix}^{\perp} \tag{42}$$

where $[\cdot]^{\perp}$ is a matrix with the same row space as $[\cdot]$, and the last term in Eqs. (41) and (42) is the residual term. Using the residual term, Eq. (42) can be expressed as follows:

$$\begin{bmatrix} \boldsymbol{\Gamma}_{i-1}^{\dagger}\mathbf{Z}_{i+1} \\ \mathbf{Y}_{i|i} \end{bmatrix} = \begin{bmatrix} \mathbf{K}_{11} & \mathbf{K}_{12} \\ \mathbf{K}_{21} & \mathbf{K}_{22} \end{bmatrix} \begin{bmatrix} \boldsymbol{\Gamma}_i^{\dagger}\mathbf{Z}_i \\ \mathbf{U}_{i|2i-1} \end{bmatrix} + \begin{bmatrix} \rho_1 \\ \rho_2 \end{bmatrix}. \tag{43}$$

To minimize the residual of the above equation, the system matrices **A** and **C** can be obtained using the least squares method as follows [11]:

$$\min_{\mathbf{K}_{11},\mathbf{K}_{12},\mathbf{K}_{21},\mathbf{K}_{22}} \left\| \begin{bmatrix} \boldsymbol{\Gamma}_{i-1}^{\dagger}\mathbf{Z}_{i+1} \\ \mathbf{Y}_{i|i} \end{bmatrix} - \begin{bmatrix} \mathbf{K}_{11} & \mathbf{K}_{12} \\ \mathbf{K}_{21} & \mathbf{K}_{22} \end{bmatrix} \begin{bmatrix} \boldsymbol{\Gamma}_i^{\dagger}\mathbf{Z}_i \\ \mathbf{U}_{i|2i-1} \end{bmatrix} \right\|_{\mathbf{F}}^2 \tag{44}$$

$$\mathbf{A} \leftarrow \mathbf{K}_{11} \tag{45}$$

$$\mathbf{C} \leftarrow \mathbf{K}_{21} \tag{46}$$

$$\begin{bmatrix} \mathbf{Q}^s & \mathbf{S}^s \\ (\mathbf{S}^s)^T & \mathbf{R}^s \end{bmatrix} \leftarrow \frac{1}{j} \begin{bmatrix} \rho_1\rho_1^T & \rho_1\rho_2^T \\ \rho_2\rho_1^T & \rho_2\rho_2^T \end{bmatrix} \tag{47}$$

Equation (47) is the estimated covariance matrix of the stochastic system. By linearly optimizing Eq. (43) using the least squares method, the variable matrices on the left and right sides can be expressed using Eq. (32) and the singular value decomposition result as follows:

$$\begin{bmatrix} \boldsymbol{\Gamma}_i^{\dagger}\mathbf{Z}_i \\ \mathbf{U}_{i|2i-1} \end{bmatrix} = \begin{bmatrix} \boldsymbol{\Sigma}_1^{-1/2}\mathbf{U}_1^T\mathbf{R}_{5:6,1:4} \\ \mathbf{R}_{2:3,1:4} \end{bmatrix} \mathbf{Q}_{1:4}^T \tag{48}$$

$$\begin{bmatrix} \boldsymbol{\Gamma}_{i-1}^{\dagger}\mathbf{Z}_{i+1} \\ \mathbf{Y}_{i|i} \end{bmatrix} = \begin{bmatrix} \boldsymbol{\Sigma}_1^{-1/2}\begin{pmatrix} \mathbf{U}_1 \\ - \end{pmatrix}^{\dagger}\mathbf{R}_{6:6,1:5} \\ \mathbf{R}_{5:5,1:5} \end{bmatrix} \mathbf{Q}_{1:5}^T \tag{49}$$

Equations (48) and (49) are substituted into Eq. (44) to obtain the following equation:

$$\min_{\mathbf{K}} \left\| \begin{bmatrix} \boldsymbol{\Sigma}_1^{-1/2}\begin{pmatrix} \mathbf{U}_1 \\ - \end{pmatrix}^{\dagger}\mathbf{R}_{6:6,1:4} \\ \mathbf{R}_{5:5,1:4} \end{bmatrix} - \mathbf{K} \begin{bmatrix} \boldsymbol{\Sigma}_1^{-1/2}\mathbf{U}_1^T\mathbf{R}_{5:6,1:4} \\ \mathbf{R}_{2:3,1:4} \end{bmatrix} \right\|_{\mathbf{F}}^2 \tag{50}$$

where **K** is a block matrix consisting of $\mathbf{K}_{ij}(i = 1,2, j = 1,2)$, and system matrices **A** and **C** can be calculated using Eqs. (45) and (46). These system matrices can be used to obtain the mode shape, natural frequency, and damping ratio for each mode.

Estimation of Modal Properties Using the Identified System Matrices

The system matrices **A**, **B**, and **C** obtained using N4SID can be used to calculate the structure's mode shape, natural frequency, and mode damping ratio. If the identification matrix of the system matrix **A** is $\widehat{\mathbf{A}}$, then an eigenvalue problem of $\widehat{\mathbf{A}}$ can be formulated as follows:

$$\widehat{\mathbf{A}}\mathbf{v} = \lambda\mathbf{v} \tag{51}$$

The above eigenvalue problem can be solved to obtain the following eigenvalue and eigenvector:

$$\boldsymbol{\Lambda} = \begin{bmatrix} \lambda_1 \\ \lambda_2 \\ \vdots \\ \lambda_n \end{bmatrix} \tag{52}$$

$$\boldsymbol{\Phi} = \begin{bmatrix} \mathbf{v}_1 & \mathbf{v}_2 & \cdots & \mathbf{v}_n \end{bmatrix} \tag{53}$$

Using these eigenvalue and eigenvector, the natural frequency and mode damping ratio of the target structure can be calculated as follows:

$$\omega_i = \left|\lambda_{c(i)}\right|, \tag{54}$$

$$\zeta_i = \frac{\mathrm{Re}(\lambda_{c(i)})}{\left|\lambda_{c(i)}\right|}, \tag{55}$$

where $\lambda_{c(i)}$ is calculated using the eigenvalue of Eq. (52) as follows:

$$\lambda_{c(i)} = \frac{\ln(\lambda_i)}{dt}. \tag{56}$$

Finally, using the identification matrix $\widehat{\mathbf{C}}$ of the output matrix **C**, the mode shape of the structure is obtained as follows:

$$\mathbf{y} = \widehat{\mathbf{C}}\mathbf{x} \tag{57}$$

where **x** is the eigenvector in Eq. (53).

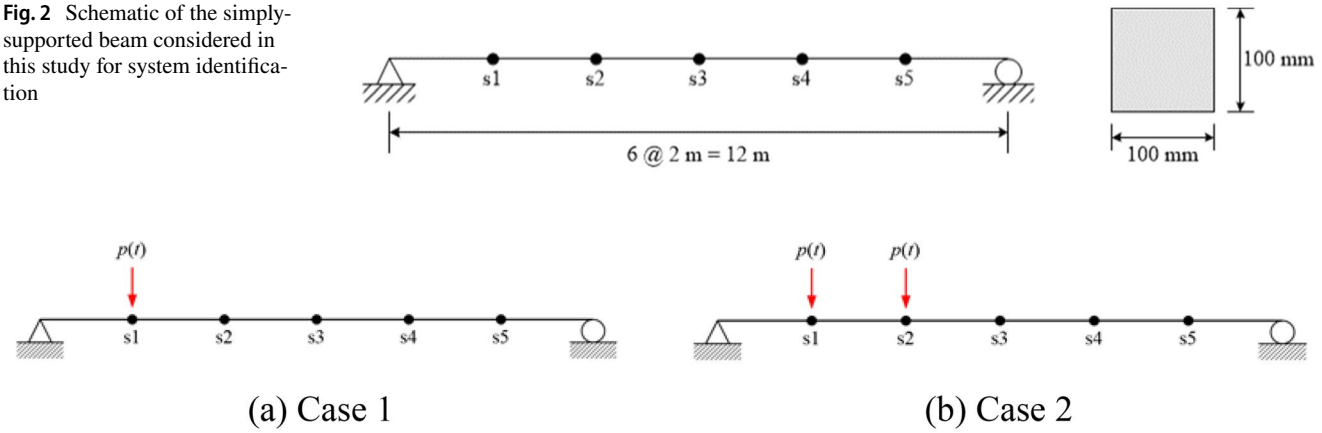

Fig. 2 Schematic of the simply-supported beam considered in this study for system identification

Fig. 3 Two cases of the impact load applied to the simply-supported beam

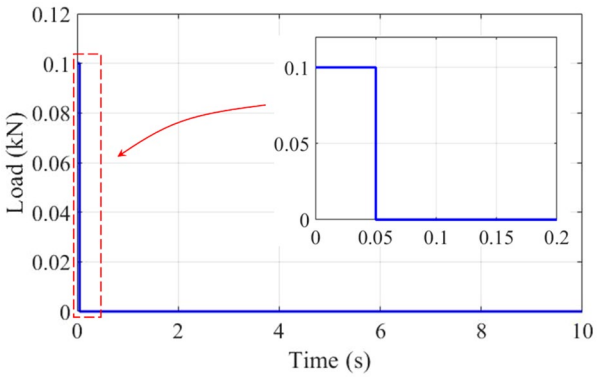

Fig. 4 Time history of the impact load

Numerical examples

In this section, we explain the calculation of the modal characteristics of a simply supported beam and cantilever beam using the presented N4SID algorithm; then, we evaluate the accuracy of the results via comparison with exact solutions. The applicability of the N4SID algorithm for the system identification of real bridges is also assessed in this section using acceleration field measurements.

Simply-Supported Beam

The simply supported beam considered in this study is a steel beam with a length of 12m and cross-sectional area of 100mm × 100mm. As shown in Fig. 2, five sensors are arranged at intervals of 2m. The elastic modulus E, density ρ, and Poisson's ratio ν of the beam were 200GPa, 7850kg/m^3, and 0.3, respectively. The vertical displacement,

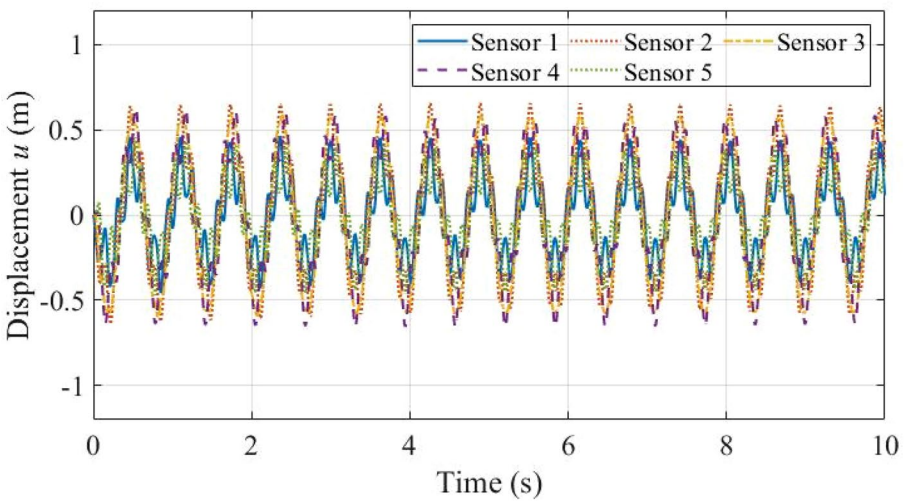

Fig. 5 Vertical displacements measured by the five sensors on the simply-supported beam in case 1

velocity, and acceleration response from sensors 1 to 5 were measured and input to the N4SID algorithm to calculate the natural frequency, mode damping ratio, and mode shape.

Loads were applied at two positions on the beam, as shown in Fig. 3, and the structural response was measured by all sensors for each case. The load was applied at the position of sensor 1 in the first case (case 1) and simultaneously at the positions of sensors 1 and 2 in the second case (case 2). Figure 4 shows the time history of this impact load. A load of 0.1 kN was applied for 0.05 s, and the response of the beam over time until $T = 10$s was measured at intervals of $\Delta t = 0.01$s. Figures 5 and 6 show the time history of the vertical displacement measured by the five sensors for each Case. This measurement response was synthesized through the dynamic analysis of the simply supported beam modeled with three-dimensional beam elements using the finite element analysis program ABAQUS.

System identification by N4SID was performed using the displacement responses at 0.1–9.78 s shown in Figs. 5 and 6. Tables 1 and 2 summarize the modal frequency estimation results obtain with the N4SID as well as the ERA results and exact solutions for comparison. In case 1, in which one impact load was used, identification was achieved up to the fourth mode, while in case 2, in which two impact loads were used, identification was possible up to the third mode. The exact solution of the modal frequency ω_n^{ex} and mode

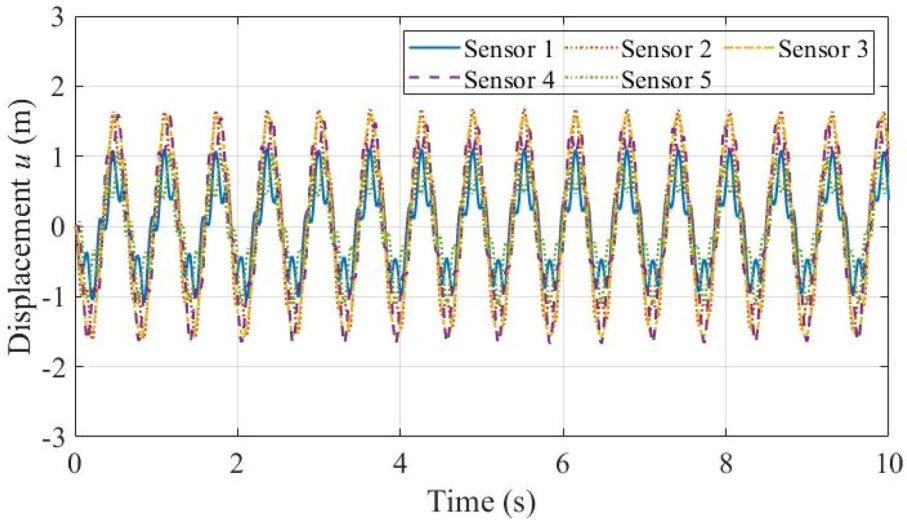

Fig. 6 Vertical displacements measured by the five sensors on the simply-supported beam in case 2

Table 1 Estimated modal properties of the simply-supported beam in case 1

Mode no	Exact solution ω_n^{ex} (rad/s)	N4SID			ERA		
		Modal frequency ω_n (rad/s)	Frequency error $\varepsilon_{\omega_n}(\%)$	$\varepsilon_{\text{MAC}}(\%)$	Modal frequency ω_n (rad/s)	Frequency error $\varepsilon_{\omega_n}(\%)$	$\varepsilon_{\text{MAC}}(\%)$
1	9.9868	10.0031	0.1634	2.99×10^{-11}	10.0031	0.1634	4.44×10^{-13}
2	39.9472	39.7567	0.4770	3.28×10^{-10}	39.7567	0.4770	6.55×10^{-13}
3	89.8813	85.4992	4.8754	1.48×10^{-6}	85.4992	4.8754	3.42×10^{-10}
4	159.7890	135.5680	15.1581	1.22×10^{0}	135.5654	15.1597	1.56×10^{-7}

Table 2 Estimated modal properties of the simply-supported beam in case 2

Mode No	Exact solution ω_n^{ex} (rad/s)	N4SID			ERA		
		Modal frequency ω_n (rad/s)	Frequency error $\varepsilon_{\omega_n}(\%)$	$\varepsilon_{\text{MAC}}(\%)$	Modal frequency ω_n (rad/s)	Frequency error $\varepsilon_{\omega_n}(\%)$	$\varepsilon_{\text{MAC}}(\%)$
1	9.9868	10.0031	0.1634	1.33×10^{-13}	10.0031	0.1634	2.22×10^{-12}
2	39.9472	39.7567	0.4770	1.92×10^{-11}	39.7566	0.4770	6.86×10^{-12}
3	89.8813	85.4992	4.8754	2.60×10^{-7}	85.4992	4.8754	5.02×10^{-9}
4	159.7890	138.6878	13.2057	8.35×10^{-1}	137.3263	14.0577	6.30×10^{0}

shape ϕ_n^{ex} for the simply supported beam can be calculated as follows:

$$\omega_n^{\text{ex}} = \frac{(n\pi)^2}{L^2}\sqrt{\frac{EI}{\rho A}}, \tag{58}$$

$$\phi_n^{\text{ex}} = \sin\left(\frac{n\pi}{L}x\right), \tag{59}$$

where n is the mode order, L is the beam length, I is the second cross-sectional moment of inertia, and A is the cross-sectional area. The error of the mode shape and natural frequency can be calculated using the exact solution as follows:

$$\varepsilon_{\omega_n} = \left|1 - \frac{\omega_n}{\omega_n^{\text{ex}}}\right|, \tag{60}$$

$$\varepsilon_{\text{MAC}} = 1 - \frac{\left|\boldsymbol{\phi}_n^T \boldsymbol{\phi}_n^{\text{ex}}\right|}{\sqrt{\left(\boldsymbol{\phi}_n^T \boldsymbol{\phi}_n\right)\left(\left(\boldsymbol{\phi}_n^{\text{ex}}\right)^T \boldsymbol{\phi}_n^{\text{ex}}\right)}}, \tag{61}$$

where $\boldsymbol{\phi}_n^{\text{ex}}$ is the discrete n th mode vector, and ε_{MAC} is the modal assurance criterion (MAC).

From Tables 1 and 2, it can be seen that the natural frequency and mode shape calculated using N4SID were close to the exact solution. The N4SID results were nearly identical to those obtained using ERA. There is a very small difference in the identification value of the modal frequency in

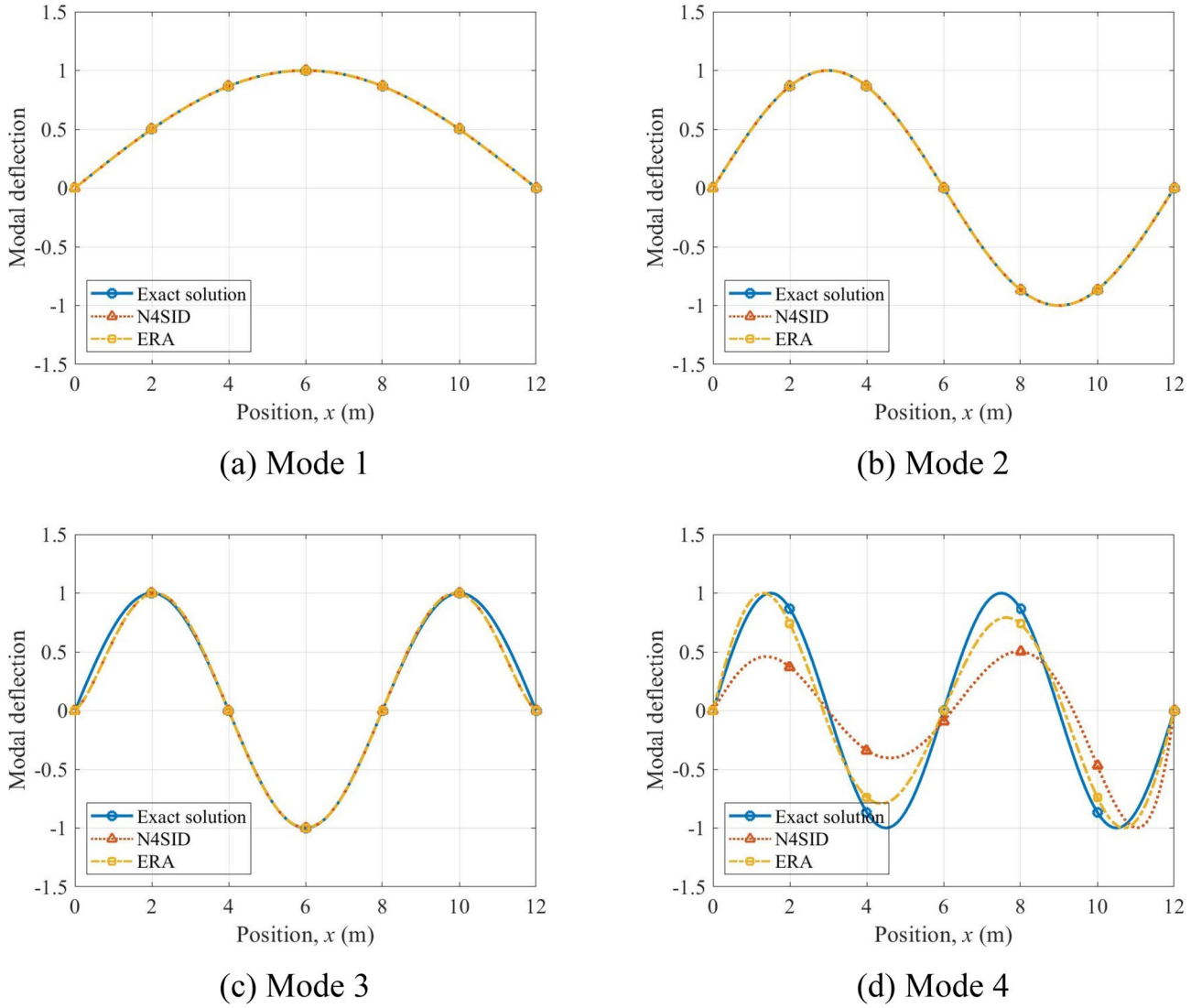

Fig. 7 Mode shapes of the simply-supported beam identified in case 1

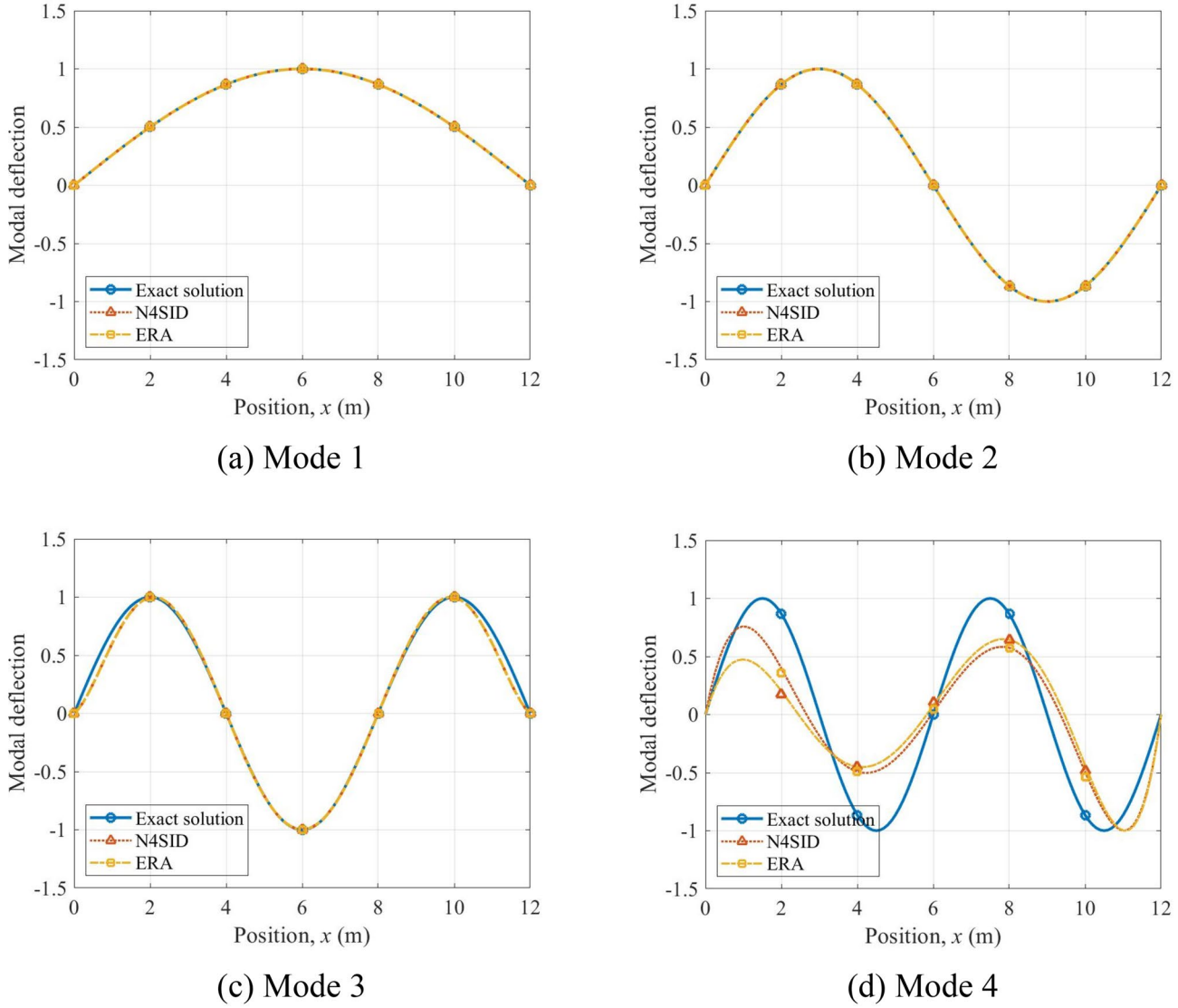

Fig. 8 Mode shapes of the simply-supported beam identified in case 2

case 1 and case 2, and the value of $\varepsilon_{\mathrm{MAC}}$, which indicates the error of the modal shape, is also very small in the lower mode. The error of the modal frequency and mode shape is known to increase as the mode order increases. In case 1, the first and second modes showed high accuracy with a natural frequency error of less than 1%, while the error of the fourth mode was approximately 15%. The error results for each mode were similar in case 2. Figure 7 shows the mode shapes identified using N4SID and ERA in case 1, and Fig. 8 shows the mode shapes in case 2. In case 1, the fourth mode shape reconstructed using ERA is closer to the exact solution than the mode shape reconstructed using N4SID. However, in case 2, the N4SID result is closer to the exact solution than ERA, as shown in Table 2 and Fig. 8d. Note that only six sensors have been used in this example. If more data points were used, the system identification methods could identify higher modes, and the identified natural frequencies and mode shapes would be more accurate.

Figure 9 shows a stability chart describing the identification results of the modal frequency of the simply supported beam. The natural frequencies identified with the highest frequency indicate the first to fourth modes; the fifth mode was not identified in this example, in which only five sensors were used. N4SID clearly identified the first to fourth modes, whereas the identification of the fourth mode by the ERA is relatively unclear.

To compare the accuracy of the modal identification results according to the type of measurement data, we conducted system identification using a 1–2 s interval of displacement, velocity, and acceleration response at each sensor

position of the simply supported beam. Figure 10 shows the error in the modal frequency and mode shape according to the type of measurement data. Although the types of measurement data differed, the identification results of the natural frequency and mode shape were nearly identical when there was no noise. The error in the mode shape of the first and second mode was the smallest when using displacement data, but the error in the higher modes was the smallest when using acceleration data. The result indicates that using acceleration data is more suitable for identifying higher modes than displacement data. Nevertheless, the error when using displacement or velocity was sufficiently small for all four modes.

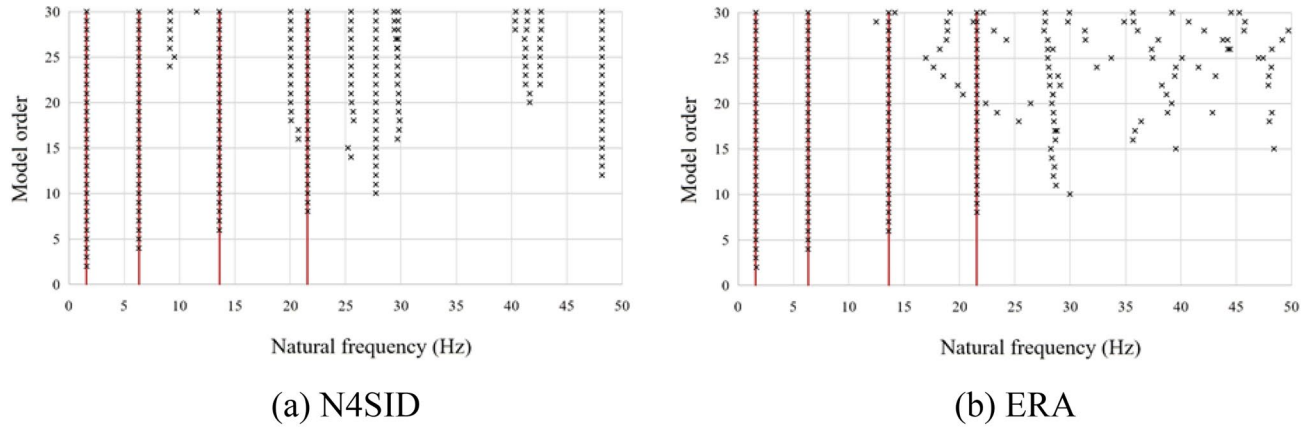

Fig. 9 Stability chart in the modal identification of the simply-supported beam (case 1)

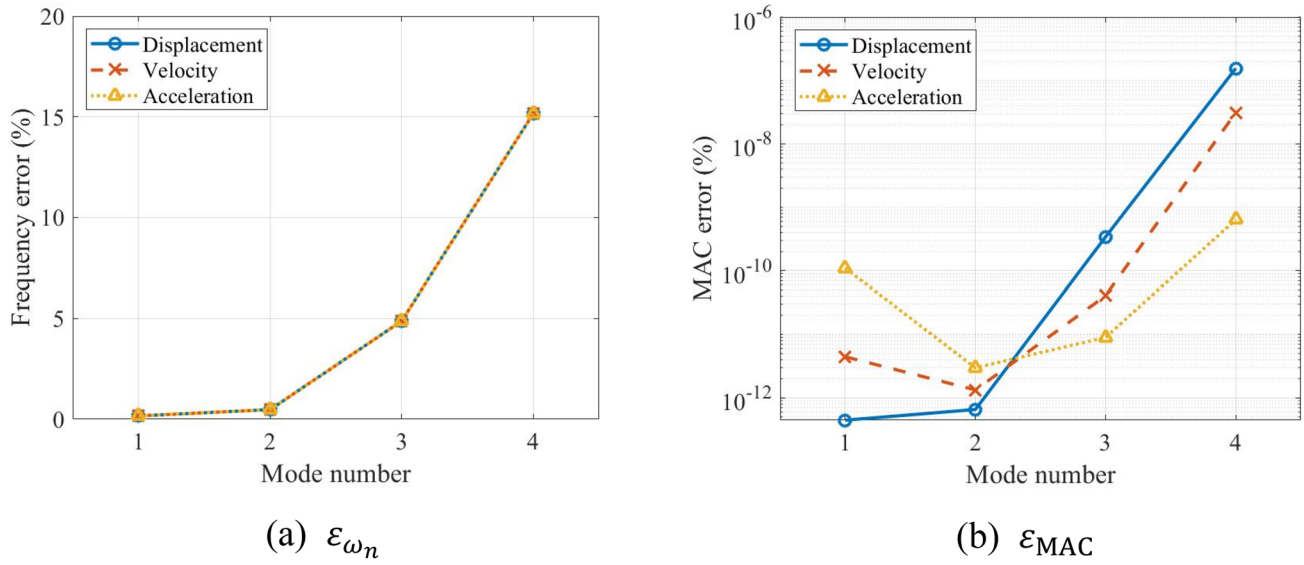

Fig. 10 Error in natural frequency and mode shape according to the type of measurement data in case 1

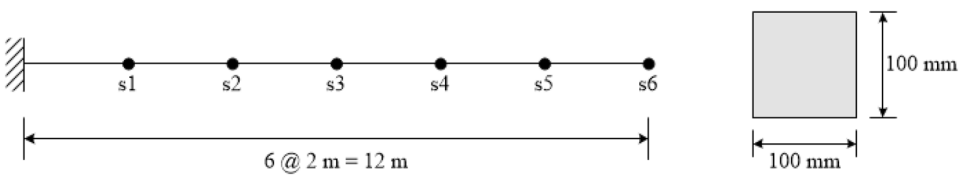

Fig. 11 Schematic of the cantilever beam used in this study for system identification

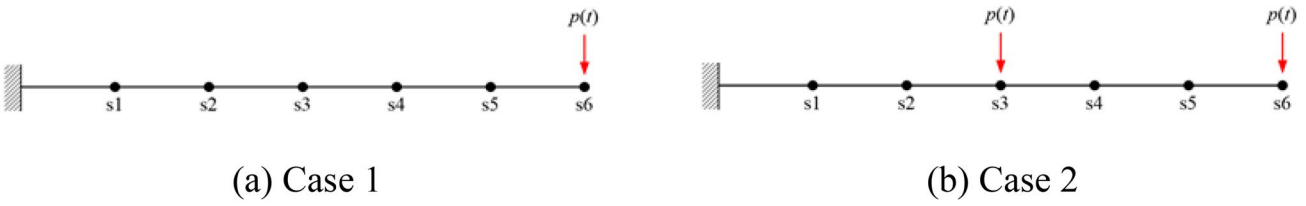

Fig. 12 Two impact load cases applied to the cantilever beam

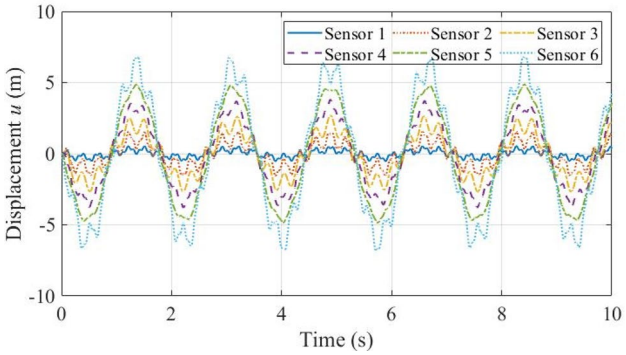

Fig. 13 Vertical displacements measured at six sensor locations of the cantilever beam in case 1

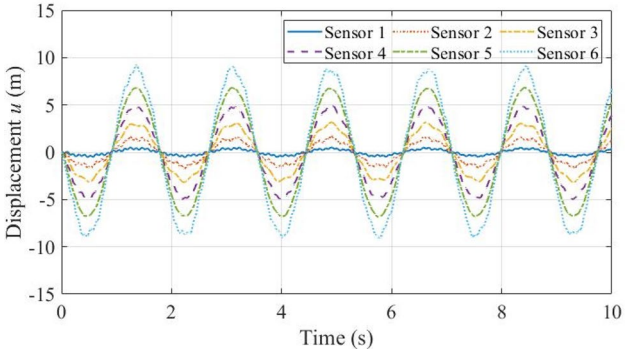

Fig. 14 Vertical displacements measured at six sensor locations of the cantilever beam in case 2

Cantilever Beam

To verify the effectiveness of N4SID, we conducted another experiment with a steel cantilever beam with a length of 12 m and a cross-sectional area of 100mm × 100mm, as shown in Fig. 11. The elastic modulus, density, and Poisson's ratio of this beam were the same as those of the simply supported beam described in Sect. 5.1. A total of six sensors were arranged at 2 m intervals, and the vertical displacement caused by a given load was measured by each sensor.

Two cases were considered for the input load to induce vibration in the beam, as shown in Fig. 12. The load was applied at the position of sensor 6 in the first case (case 1) and simultaneously at the positions of sensors 3 and 6 in the second case (case 2). The same load shown in Fig. 4 was applied here. Figures 13 and 14 show the time history of the vertical displacement measured by the six sensors for each case.

System identification by N4SID was performed with the displacement responses of Figs. 13 and 14 between 0.1 and 8.78 s. Tables 3 and 4 summarize the modal frequency estimated by N4SID as well as ERA and the exact solutions for comparison. The exact solution of the modal frequency ω_n^{ex} and mode shape ϕ_n^{ex} for the cantilever beam can be calculated as follows:

$$\omega_n^{\text{ex}} = \left(a_n L\right)^2 \sqrt{\frac{EI}{\rho A L^4}}, \tag{62}$$

Table 3 Estimated modal properties of the cantilever beam in case 1

Mode No	Exact solution ω_n^{ex} (rad/s)	N4SID			ERA		
		Modal frequency ω_n (rad/s)	Frequency error $\varepsilon_{\omega_n}(\%)$	$\varepsilon_{\text{MAC}}(\%)$	Modal frequency ω_n (rad/s)	Frequency error $\varepsilon_{\omega_n}(\%)$	$\varepsilon_{\text{MAC}}(\%)$
1	3.5578	3.5576	3.17×10^{-3}	2.65×10^{-8}	3.5574	8.64×10^{-3}	1.10×10^{-8}
2	22.2962	22.2849	5.07×10^{-2}	6.40×10^{-6}	22.2846	5.17×10^{-2}	1.81×10^{-6}
3	62.4299	62.3412	1.42×10^{-1}	6.16×10^{-6}	62.3428	1.39×10^{-1}	1.33×10^{-5}
4	121.5163	122.2316	5.89×10^{-1}	1.96×10^{-1}	121.9942	3.93×10^{-1}	1.06×10^{-1}
5	202.2334	200.9477	6.36×10^{-1}	4.56×10^{0}	200.8662	6.76×10^{-1}	4.43×10^{0}

Table 4 Estimated modal properties of the cantilever beam in case 2

Mode No	Exact solution ω_n^{ex} (rad/s)	N4SID			ERA		
		Modal frequency ω_n (rad/s)	Frequency error $\varepsilon_{\omega_n}(\%)$	$\varepsilon_{MAC}(\%)$	Modal frequency ω_n (rad/s)	Frequency error $\varepsilon_{\omega_n}(\%)$	$\varepsilon_{MAC}(\%)$
1	3.5578	3.5570	1.98×10^{-2}	1.14×10^{-8}	3.5570	1.98×10^{-2}	1.11×10^{-8}
2	22.2962	22.1817	5.14×10^{-1}	1.14×10^{-6}	22.1817	5.14×10^{-1}	1.60×10^{-6}
3	62.4299	60.2217	3.54×10^{0}	9.10×10^{-6}	60.2217	3.54×10^{0}	6.01×10^{-6}
4	121.5163	108.5096	1.07×10^{1}	3.99×10^{-2}	108.5076	1.07×10^{1}	3.98×10^{-2}
5	202.2334	135.7914	3.29×10^{1}	6.27×10^{0}	155.4823	2.31×10^{1}	4.58×10^{0}

$$\phi_n^{ex} = \cosh(a_n x) - \cos(a_n x) - \frac{\cos(a_n L) - \cosh(a_n L)}{\sin(a_n L) - \sinh(a_n L)}\left(\sinh(a_n x) - \sin(a_n x)\right), \tag{63}$$

where a_n can be calculated by satisfying Eq. (64), which indicates the boundary condition of the cantilever beam.

$$\cosh(a_n L) - \cos(a_n L) + 1 = 0 \tag{64}$$

As before, the error of the identified natural frequency and mode shape is calculated using Eqs. (60) and (61).

From Tables 3 and 4, it can be seen that the natural frequency and mode shape calculated using N4SID were close to the exact solution. The N4SID results were nearly identical to those obtained using ERA. For the cantilever beam, the identification value of the modal frequency obtained using a single load was more accurate than that obtained using two loads. In case 1, both N4SID and ERA showed a natural frequency error of less than 1% in the first to fifth modes, with the ERA and N4SID showing more accuracy in the fourth and fifth modes, respectively. In case 2, the natural frequency error of the first and second modes was smaller than 1%, while the error of the fourth and fifth modes was greater than 10% and 30%, respectively. This demonstrates that it is more advantageous to use a single load rather than multiple loads when performing system identification using an input load. The value of ε_{MAC}, which represents the error of the mode shape, barely differed between the two cases. Figures 15 and 16 show the mode shape of the cantilever beam identified using N4SID and ERA in case 1 and case 2, respectively.

Figure 17 shows a stability chart describing the identification results of the modal frequency of the cantilever beam. The natural frequencies identified with the highest frequency indicate the first to fifth modes; in this example, in which only six sensors were used, modes above the fifth were not identified. While both N4SID and ERA identify five modal frequencies well, N4SID identifies natural frequencies in higher modes more consistently than ERA.

Full-Scale Bridge with Field Measurement Data

Finally, vibration data were used to estimate the modal characteristics and damping ratio of the Geumdang Bridge, which is located in Yeoju-si, Gyeonggi-do, Korea. It is a prestressed concrete I-girder bridge with a total length of 270 m and width of 12.1 m. It has a total of nine spans, and the length of one span is 30 m. The vibrations were measured with accelerometers arranged at 5 m intervals in the 30 m segment between the abutment and the first pier. The data measurement time was 125 min, and the time step was 0.01 s. The measurement data were limited to the range of 2–30 Hz using a band-pass filter, and system identification was performed using these data. Figure 18 shows a photograph of the Geumdang Bridge investigated in this study and the 15 accelerometers installed in one segment. Figure 19 shows the time history and frequency spectrum of the data measured by accelerometers 6 and 8.

Using the proposed method, the natural frequency, mode shape, and modal damping ratio of the Geumdang Bridge could be identified up to the third mode. Figures 20 and 21 show the mode shape of the Geumdang Bridge obtained using N4SID and ERA, respectively. It can be seen that mode 1 is similar to a half-sinusoidal symmetric mode, and mode 3 is similar to a sinusoidal antisymmetric mode. Mode 2 was evaluated as a mode with torsional behavior.

Table 5 shows the identification results of the modal frequency and modal damping ratio of the Geumdang Bridge up to the third mode. From the table, it can be seen that the modal frequencies identified by N4SID and ERA were similar, but the modal damping ratio identified by N4SID

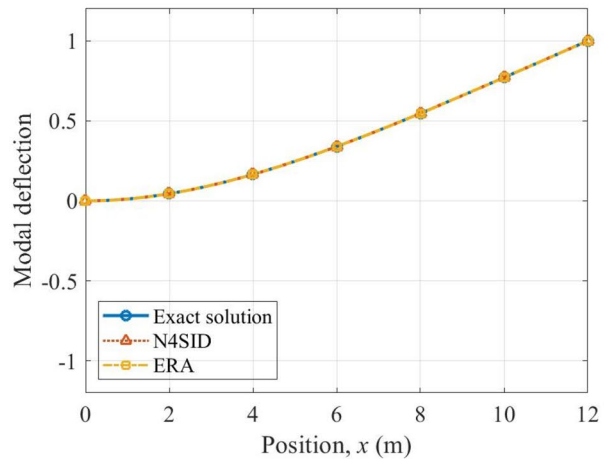

(a) Mode 1

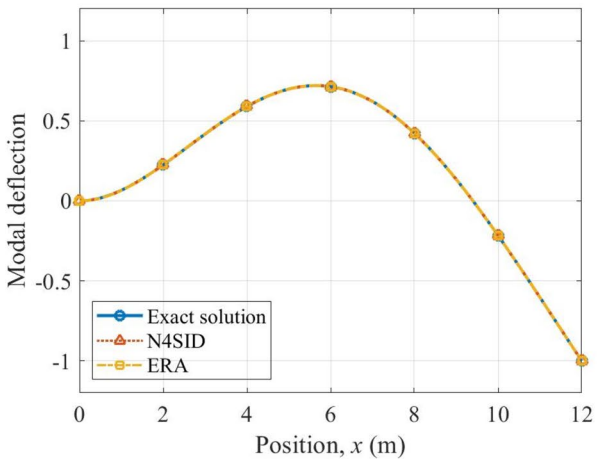

(b) Mode 2

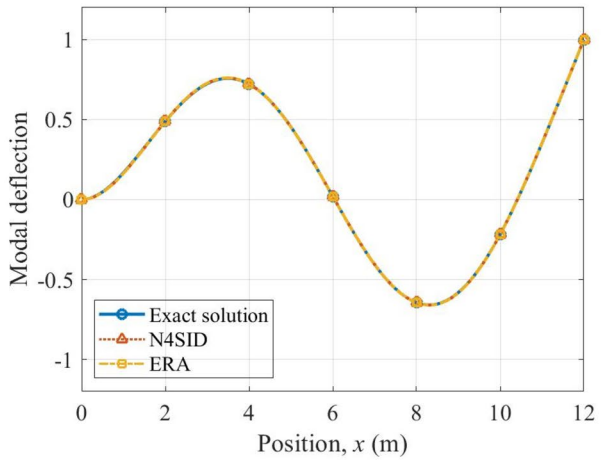

(c) Mode 3

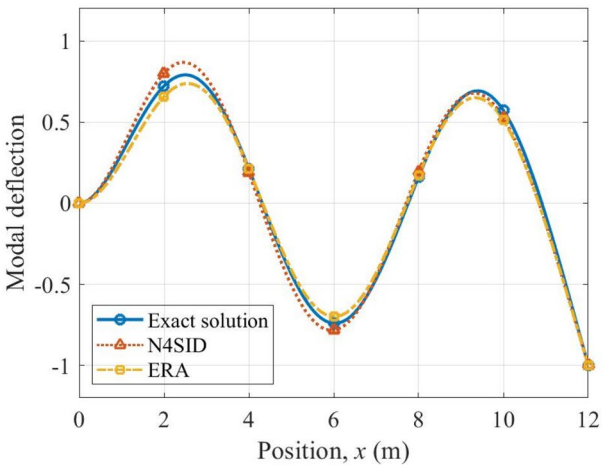

(d) Mode 4

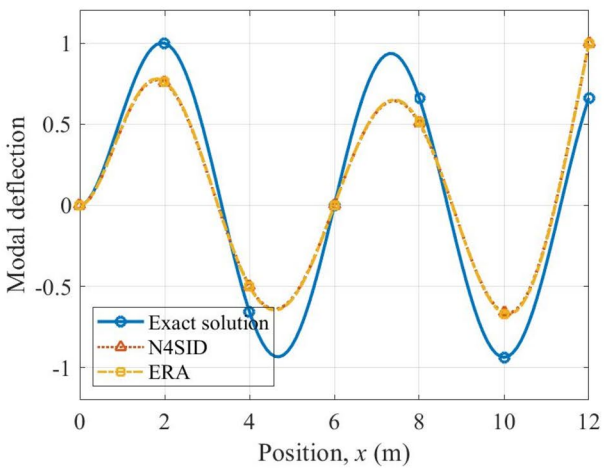

(e) Mode 5

Fig. 15 Mode shapes of the cantilever beam identified in case 1

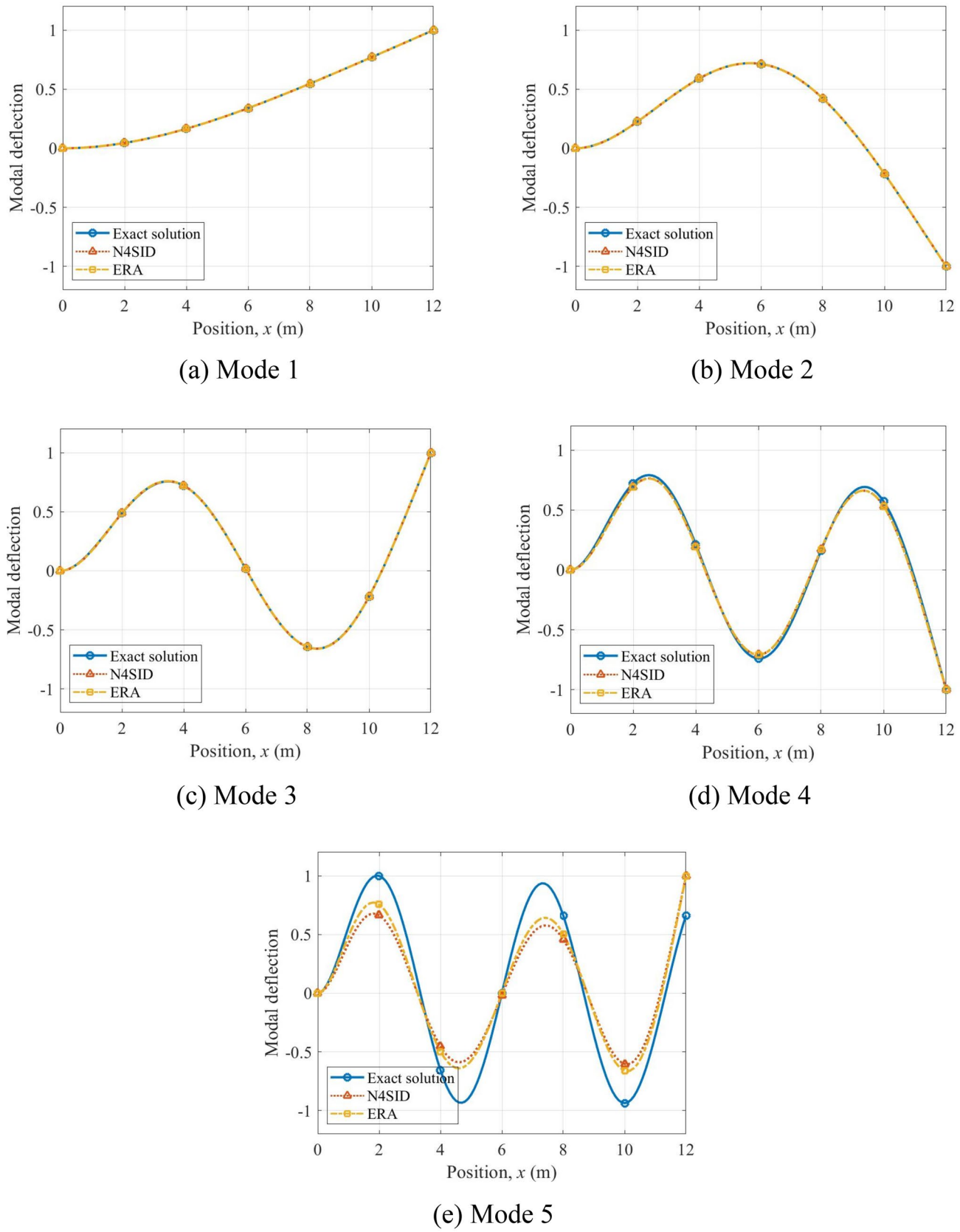

Fig. 16 Mode shapes of the cantilever beam identified in case 2

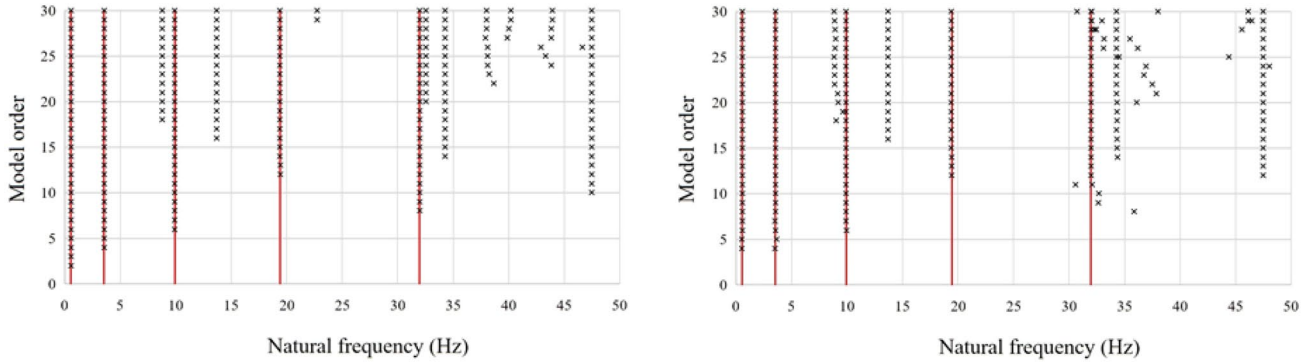

(a) N4SID (b) ERA

Fig. 17 Stability chart in the modal identification of the cantilever beam (case 1)

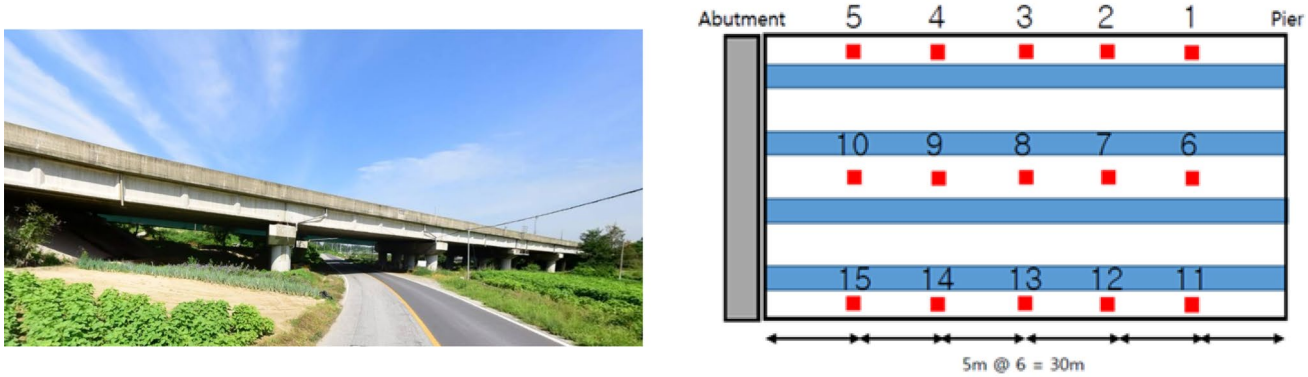

(a) Side photo (b) Sensor placement

Fig. 18 Geumdang Bridge at Yeoju, Gyeonggi-do, Korea

was greater than that estimated by ERA. Given that the Geumdang Bridge segment investigated in this study is connected to the abutment, the modal damping ratio identified by N4SID is likely to be more practical than that identified by ERA. Figure 22 is a stability chart showing the identification results of the modal frequency of the Geumdang Bridge obtained using N4SID. The identification results of the modal frequency are unclear compared to those of the cantilever beam and simply supported beam using synthetic data. Nevertheless, they indicate that system identification can be performed using only ambient vibration data without input loads and that this system identification technique has potential application to the structural health monitoring of various infrastructures.

Conclusions

This study evaluated the applicability of N4SID in the identification of the dynamic characteristics of bridge structures at the element and system levels. The N4SID method constructs a Hankel matrix from the input and measurement data, applies QR factorization and singular value decomposition to construct a Kalman state vector, and then optimizes the state-space system matrix. The dynamic characteristics of a simply supported beam and cantilever beam were estimated using a small number of measurement data. The natural frequencies and mode shapes were accurately identified up to the fourth and fifth modes. While system identification

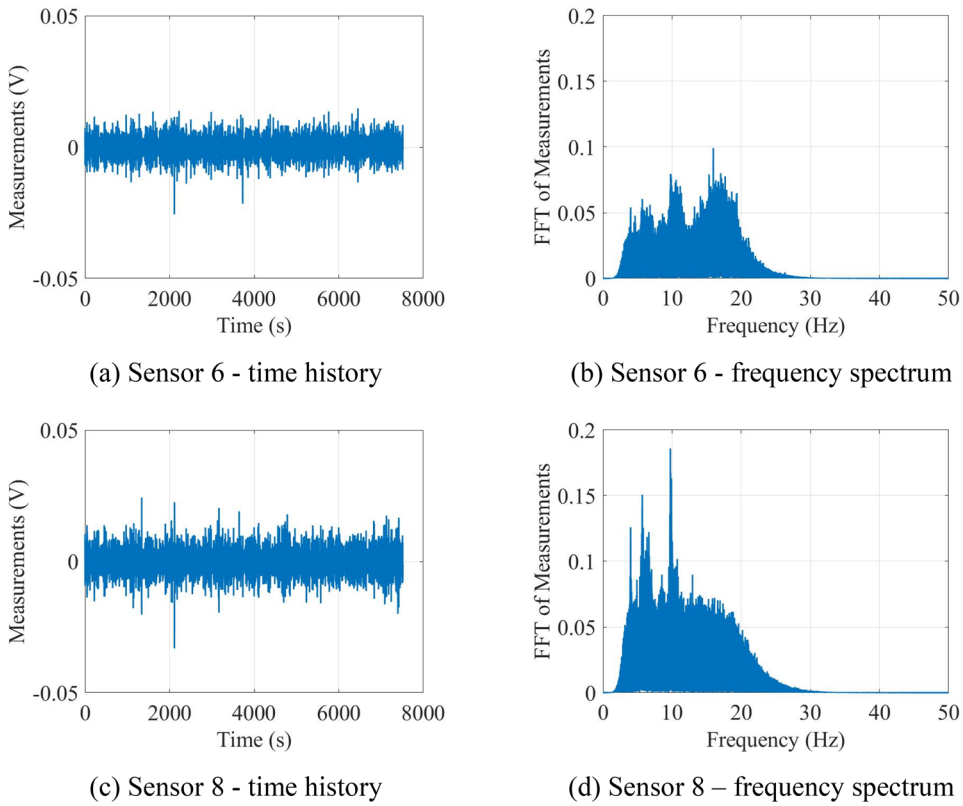

Fig. 19 Acceleration data of the Geumdang Bridge measured by sensors 6 and 8

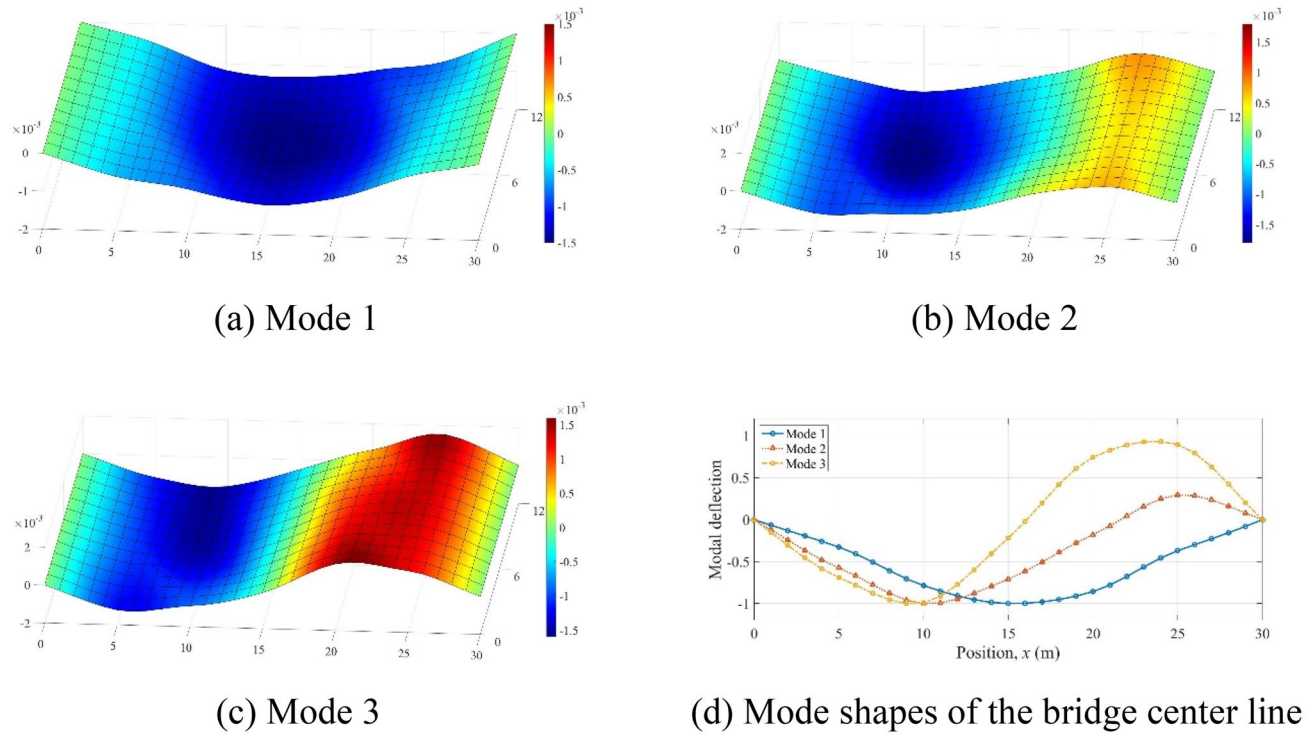

Fig. 20 Mode shapes of the Geumdang Bridge estimated by N4SID

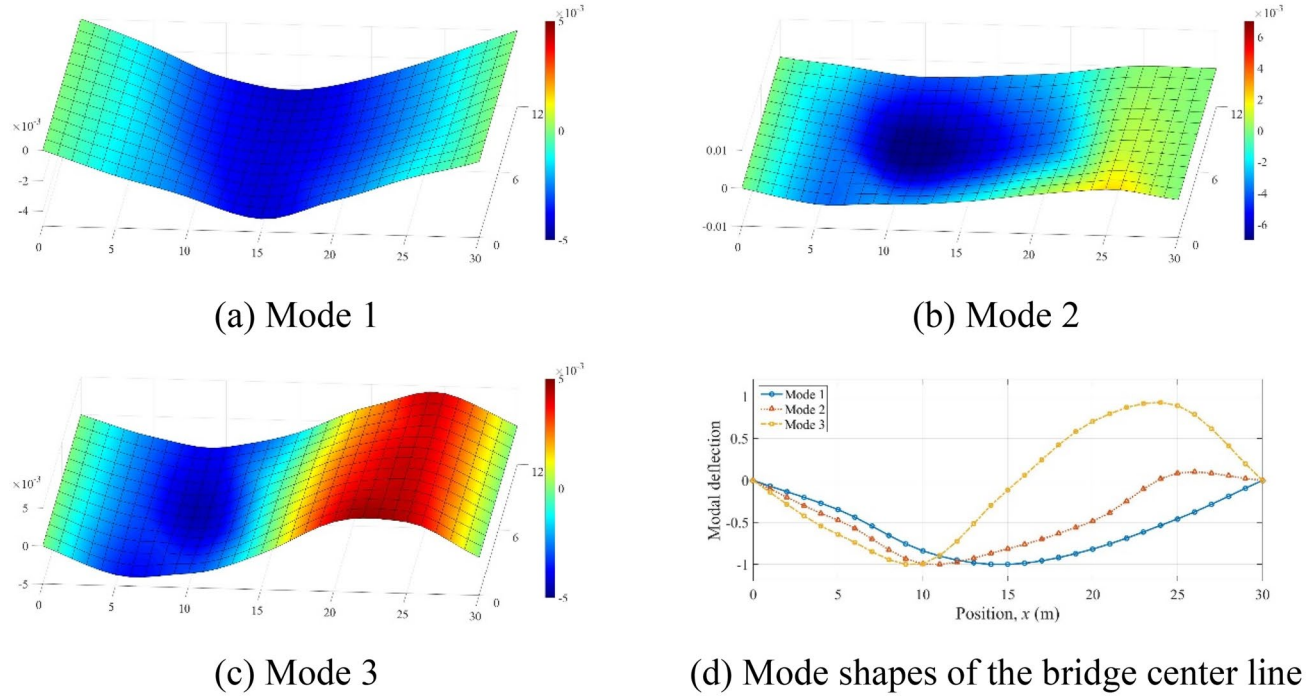

Fig. 21 Mode shapes of the Geumdang Bridge estimated by ERA

Table 5 Estimated modal frequency and damping ratio of the Geumdang Bridge

Mode no	N4SID		ERA	
	Modal frequency f_n (Hz)	Modal damping ratio ζ_n	Modal frequency f_n (Hz)	Modal damping ratio ζ_n
1	5.933	0.1470	5.903	0.0068
2	10.128	0.1530	10.177	0.0004
3	15.786	0.0626	16.033	0.0017

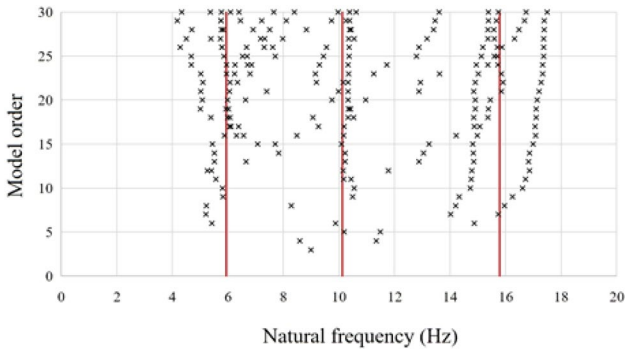

Fig. 22 Stability chart in the modal identification of the Geumdang Bridge

was possible using multiple input loads, the accuracy of system identification was higher when only one input load was used. The error in the mode shape was smaller when using acceleration data than when using displacement or velocity data. However, even though the types of measurement data differed, the difference in the identified natural frequencies and mode shapes was not large when there was no noise. Furthermore, using the acceleration data measured from a real bridge, the modal characteristics and damping ratio of the bridge were estimated accurately. The stability chart of N4SID shows that the system identification of bridge structures is possible using only a limited number of ambient vibration data without an input load.

Acknowledgements This research was funded by Korea Institute of Civil Engineering and Building Technology, grant from a Strategic Research Project (Smart Monitoring System for Concrete Structures Using FRP Nerve Sensor). This support is greatly appreciated.

References

1. M. Chang, Application studies on structural modal identification toolsuite for seismic response of shear frame structure. J. Earthq. Eng. Soc. Korea **22**(3), 201–210 (2018)
2. M. Chang, R.L. Leonard, S.N. Pakzad, *Structural Modal Identification Toolsuite (SMIT) User's Guide* (Lehigh University, Bethlehem, 2012)

3. M. Chang, S.N. Pakzad, Modified natural excitation technique for stochastic modal identification. J. Struct. Eng. (2012). https://doi.org/10.1061/(ASCE)ST.1943-541X.0000559
4. B.L. Ho, R.E. Kalman, Effective construction of linear, state-variable models from input/output functions. Regelungstechnik **14**(12), 545–548 (1966)
5. James, G. H. III, Carne, T. G., Lauffer, J. P. (1993). The natural excitation technique (NExT) for modal parameter extraction from operating wind turbines. SAND92–1666, UC261, Sandia National Laboratories.
6. J.N. Juang, *Applied System Identification* (Prentice Hall, Englewood Cliffs, 1994)
7. J.N. Juang, R.S. Pappa, An eigensystem realization algorithm for modal parameter identification and model reduction. J. Guid. Control Dyn. **8**(5), 620–627 (1985)
8. J. Kim, J.P. Lynch, Subspace system identification of support-excited structures—part I: theory and black-box system identification. Earthq. Eng. Struct. Dyn. **41**(15), 2235–2251 (2012)
9. B. Peeters, G. De Roeck, Reference-based stochastic subspace identification for output-only modal analysis. Mech. Syst. Signal Process. **13**(6), 855–878 (1999)
10. H. Shokravi, H. Shokravi, N. Bakhary, S.S.R. Koloor, M. Petru, Health monitoring of civil infrastructures by subspace system identification method: an overview. Appl. Sci. **10**, 2786 (2020). https://doi.org/10.3390/app10082786
11. P. Van Overschee, B. De Moor, N4SID: subspace algorithms for the identification of combined deterministic-stochastic systems. Automatica **30**(1), 75–93 (1994)